Hindawi
International Journal of Aerospace Engineering
Volume 2021, Article ID 9952209, 14 pages
https://doi.org/10.1155/2021/9952209

Research Article

Investigations on Internal Ballistic Characteristics of Pasty Propellant Rocket Engine

Xinyou Shan, Yingkun Li, Xiong Chen, Yan Wu, Yong He, and Weixuan Li

School of Mechanical Engineering, Nanjing University of Science and Technology, 210094 Nanjing, China

Correspondence should be addressed to Xiong Chen; chenxiongnjust@njust.edu.cn

Received 11 March 2021; Revised 22 May 2021; Accepted 17 June 2021; Published 9 July 2021

Academic Editor: Antonio Concilio

Pasty rocket engines have broad application prospects in the aerospace field. To study the internal ballistic characteristics of the pasty propellant rocket engine, the burning surface change model of pasty propellant was built. The calculation program was developed to calculate the pressure evolution in the combustion chamber, and the experiment was carried out based on a pasty propellant rocket test system. The data calculated by the program are in good agreement with the experiment, the error of the initial pressure peak is only 4.02%, and the internal ballistic characteristics of the rocket engine at each stage were analyzed detailly. The effects of ignition delay time, transport pipeline structure, free volume of the combustion chamber, mass flow rate, and flow velocity of the pasty propellant on internal ballistic characteristics of the pasty propellant rocket engine are investigated. The results indicate that when the ignition delay time increases, the pressure rises faster and the initial pressure peak increases obviously. The transport pipe diameter changes from 11.3 mm to 7.4 mm, and the initial combustion time and residual propellant combustion time decreased by 41.3% and 36.0%. The reduction of the free volume of the combustion chamber can reduce the initial pressure peak and the time to reach the equilibrium pressure. The initial pressure spike and equilibrium pressure rise with the increase of the pasty propellant flow velocity. While the ignition transient decreased with the increase of the pasty propellant flow velocity. The internal ballistic properties can be improved by reducing the ignition delay time, the diameter of the transport pipeline, and the free volume of the combustion chamber, or by increasing the mass flow rate of the pasty propellant rocket engine.

1. Introduction

The pasty propellant is a kind of fuel that has not been solidified completely and presents non-Newtonian fluid behavior with high viscosity and plasticity, which is considered to be one of the advanced chemical propulsion in the 21st century [1]. The pasty rocket engine is a reliable thrust regulation propulsion system that has many advantages, which can be used in both civilian and military applications. It has simplified construction with deeper thrust regulation and high safety in comparison with liquid rocket engines. Compared with the traditional solid rocket motor, the pasty rocket engines have advantages of repeatable start and large thrust adjustable range [2]. In the military field, pasty rocket engines can be used for attitude engines and terminal guidance correction engines for strategic missile warhead guidance, as well as kinetic energy weapon warhead engines [3]. In the aerospace field, pasty rocket engines can be used as the internal gas servo system of the rocket and the orbit-changing attitude engine of the satellite [4–6].

The pasty rocket engine operation process has been extensively investigated for decades with theoretical, numerical, and experimental studies. Kukushkin and Ivanchenko [5, 6] have achieved certain results in the theory of pasty rocket engine, rheological properties, and practical application of pasty propellant. Several types of experimental rocket engines have been designed, manufactured, and tested successfully. Song and Ye [7] proposed a theoretical model and a test engine of the pasty rocket engine, and the residual heat of the combustion chamber was used to achieve multiple pulses. Numerical simulation results showed that this method can achieve multiple ignitions of the engine. Zhang et al. [8] numerically studied the pressure drop and heat transfer of the pasty propellant flowing in the pipeline based

on two-phase flow theory. The influences of the pipe diameter and inlet velocity on the pressure drop were analyzed. Luo et al. [9] numerically simulate the working process of the solid-gelled propellant gas generator the discrete ordinates radiation model. Liu [10] designed a pasty propellant gas generator to study the start-up characteristics of the flow adjustable pasty gas generator based on gas pressure driven. In addition, many researchers have conducted a lot of studies on the atomization characteristics of gel propellant or slurry fuel through experiments, analysis, and numerical simulation. Natan and Rahimi [11] reviewed the advantages, rheological properties, and combustion behavior of the gel propellants. Douglas and Rober [12] developed a method for formulating and characterizing the properties of metalized gel propellants for the propulsion systems. Hodge et al. [13] outlined the applications, capabilities, and state-of-the-art gelled propulsion systems, and the reliability of the gel engine system was verified through actual flight tests. Turns and Mueller [14, 15] analytically and experimentally examined the secondary atomization, ignition characteristics, and combustion performance of aluminum/liquid hydrocarbon slurry propellants. The effect of solid particle content and maximum size of particle on the smallest droplet diameter that allows secondary atomization were analyzed by using applying the established droplet shell-forming model. Bondarenko et al. [16] have investigated the thermal and gas dynamics processes in the combustion chamber of prospective rocket engines using slurry fuel, and experimental and numerical results of pressure and temperature in the combustion chamber were presented. Rahimi et al. [17] formulated and characterized a type of gel propellant, and a laboratory-scale rocket engine with selected hypergolic neat-liquid and gelled bipropellant combinations was examined successfully. Cao et al. [18–20] experimentally investigated the combustion characteristics of gelled fuel formed by inorganic gallant. The results show that the combustion rate of inorganic gel fuel decreases with the increase of gellant content, and the flow characteristic research of gelled fuel was conducted numerically. However, to the best of our knowledge, the internal ballistics of pasty propellant rocket engines has not been fully investigated yet in the open literature.

In the pasty propellant rocket engine, the internal ballistics covers the time from the onset of the igniter until the pasty propellant consumes completely. During the past decades, a lot of studies have been conducted on the numerical simulations and burning surface model of the solid rocket motor internal ballistics. Yilmaz et al. [21, 22] developed a numerical approach coupled to strand burner pressure-time history to determine the burning rates of different solid propellants, and the vacuum specific impulse, density vacuum specific impulse, and solid exhaust products were examined for several propellant formulations based on the pyrophoric material triethylaluminum (TEA) using CEA thermodynamics code. Tahsini et al. [23] numerically investigated the effect of viscosity on the internal ballistics simulation of a solid rocket motor with an internal burning cylindrical grain. Greatrix [24] studied the effect of negative/-positive erosive burning on the profile of a cylindrical-grain motor numerically. Willcox et al. [25, 26] developed a new minimum distance function method to describe the 3-D burning surface geometry of the propellant grain, and internal ballistics simulations of solid rocket motors were conducted by using a one-dimensional, time-dependent single-phase compressible flow equation. Tola and Nikbay [27, 28] developed an in-house code such as a zero-dimensional internal ballistic solver and an analytical burnback solver which are implemented to compute the variation of chamber pressure and the rocket thrust transiently. Fei et al. [29] proposed a new combustion surface calculation algorithm by tracking the depression of the combustion surface of the grain to realize the combustion surface change law of arbitrary configuration of grains. In terms of propellant combustion, Yilmaz et al. [30–32] recently used CFD codes to take advantage of the correlation proposed by Beckstead and model the combustion of aluminum particles in solid rocket propellants and examined the sensitivity of the model to changes in propellant surface temperature, propellant velocity, propellant surface radiation temperature, parcel count, particle diameter, turbulent Prandtl number, and turbulent Schmidt number. Yilmaz et al. [33] also examined the heat flux to objects outside of a firing solid propellant rocket motor plume by measuring the heat flux to gages located at various locations with respect to the rocket nozzle. Hence, the calculations of internal ballistics have become an important part of the research methods on the performance of pasty propellant rocket engines.

Many studies have focused on the internal ballistics of traditional solid rocket motor with complex propellant grain geometry, whereas there have been very few reports on the internal ballistics of the pasty propellant rocket engine. It is different from the traditional solid rocket motor. The pasty propellant continuously flows into the combustor during the operation of the engine. The propellant flow velocity should be considered in the process of burning surface change. Thus, it is of great importance to develop a change model of the burning surface of the pasty propellant and to investigate the effects of several key influential parameters on internal ballistic behaviors, including the ignition delay time, transport pipeline structure, free volume of the combustion chamber, mass flow rate, and flow velocity of the pasty propellant. This paper is aimed at developing a burning surface model for the pasty rocket engine with consideration of the initial burning stage, steady burning segment, and cut-off segment, and the pasty rocket engine test system was designed and conducted to validate the burning model. The remainder of this paper is organized as follows: Section 2 revisits the governing equations of internal ballistics and derives the burning surface model. Section 3 introduces the experimental system of the pasty rocket engine. Section 4 analyzes the results of the experiment and calculations for the pasty rocket engine.

2. Mathematical Models and Numerical Procedure

2.1. Internal Ballistic Equation. A zero-dimensional internal ballistic model is often used to calculate the pressure change in the combustion chamber for a solid rocket motor [25].

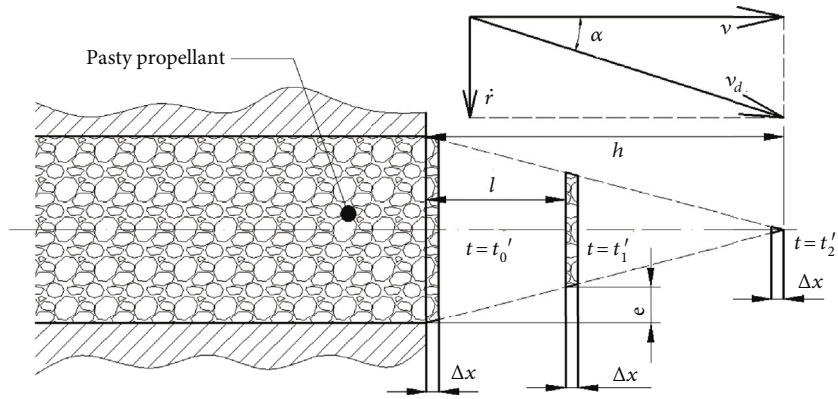

Figure 1: The selected grain change process of pasty propellant.

According to the principle of conservation of mass, the gas mass change rate in the combustion chamber is the difference between the gas generation rate $\dot{m}_b$ and the mass flow rate of the gas discharged through the nozzle $\dot{m}_0$, namely,

$$\frac{dm_r}{dt} = \dot{m}_b - \dot{m}_0, \tag{1}$$

$$\dot{m}_b = \rho_p A_b \dot{r}, \tag{2}$$

$$\dot{m}_0 = \frac{pA_t}{C^*}, \tag{3}$$

$$\dot{r} = ap^n, \tag{4}$$

$$m_r = \rho_g V_g, \tag{5}$$

where m_r represents gas quality in the combustion chamber, ρ_p is the density of the pasty propellant, A_b is the area of the burning surface, p is the pressure of the combustion chamber, A_t is the area of the nozzle throat, C^* is the characteristic velocity of the pasty propellant, and a and n represent burning rate coefficient and exponent of the propellant, respectively. ρ_g is the average density of combustion gas, and V_g is the free volume of the combustion chamber. And the meaning of all variables in this paper is listed in Nomenclature.

Differentiate the above formula (5), we can get

$$\frac{dm_r}{dt} = \rho_g \frac{dV_g}{dt} + V_g \frac{d\rho_g}{dt}. \tag{6}$$

It can be seen that the gas mass change rate in the combustion chamber consists of two parts. $\rho_g dV_g/dt$ represents the gas mass filled by the increase of the combustion chamber free volume per unit time. Because the pasty propellant is continuously added to the combustion chamber, the volume of the combustion chamber can be approximately considered constant ($dV_g/dt = 0$). $V_g d\rho_g/dt$ represents the gas quality required to change the gas density per unit time. The equation of state $\rho_g = p/(R_g T)$ is differentiated to get

$$\frac{d\rho_g}{dt} = \frac{1}{R_g T}\frac{dp}{dt} - \frac{p}{(R_g T)^2}\frac{d(R_g T)}{dt}, \tag{7}$$

where T is the temperature of the combustion gas and R_g is the gas constant. The combustion temperature keeps constant ($d(R_g T)/dt = 0$), so

$$\frac{d\rho_g}{dt} = \frac{1}{R_g T}\frac{dp}{dt}. \tag{8}$$

Substituting (8) into (6):

$$\frac{dm_r}{dt} = V_g \frac{1}{R_g T}\frac{dp}{dt}. \tag{9}$$

Substituting (9), (2), (3), and (4) into (1), we can get the zero-dimensional internal ballistic differential equation of the pasty rocket engine.

$$\frac{V_g}{R_g T}\frac{dp}{dt} = \rho_p A_b a p^n - \frac{pA_t}{C^*}. \tag{10}$$

2.2. Burning Surface Change Process of Pasty Propellant in the Combustor. In the solid rocket motor, the burning surface of the grain is derived according to the geometrical burning law [34]. Different from the traditional solid rocket motor, the pasty propellant has a flow velocity, and the volume of the combustor can be approximately considered constant. For a pasty propellant rocket engine, once the pasty propellant flows into the combustion chamber through the transport pipeline, it will be ignited and burned while being supplied. The propellant burning surface changing process can be affected by the burning surface retreat and the supply flow rate of the pasty propellant pushed by the hydraulic cylinder piston rod. Therefore, both the burning rate $\dot{r}$ and the flow velocity v of the pasty propellant have significant effects on the burning surface change.

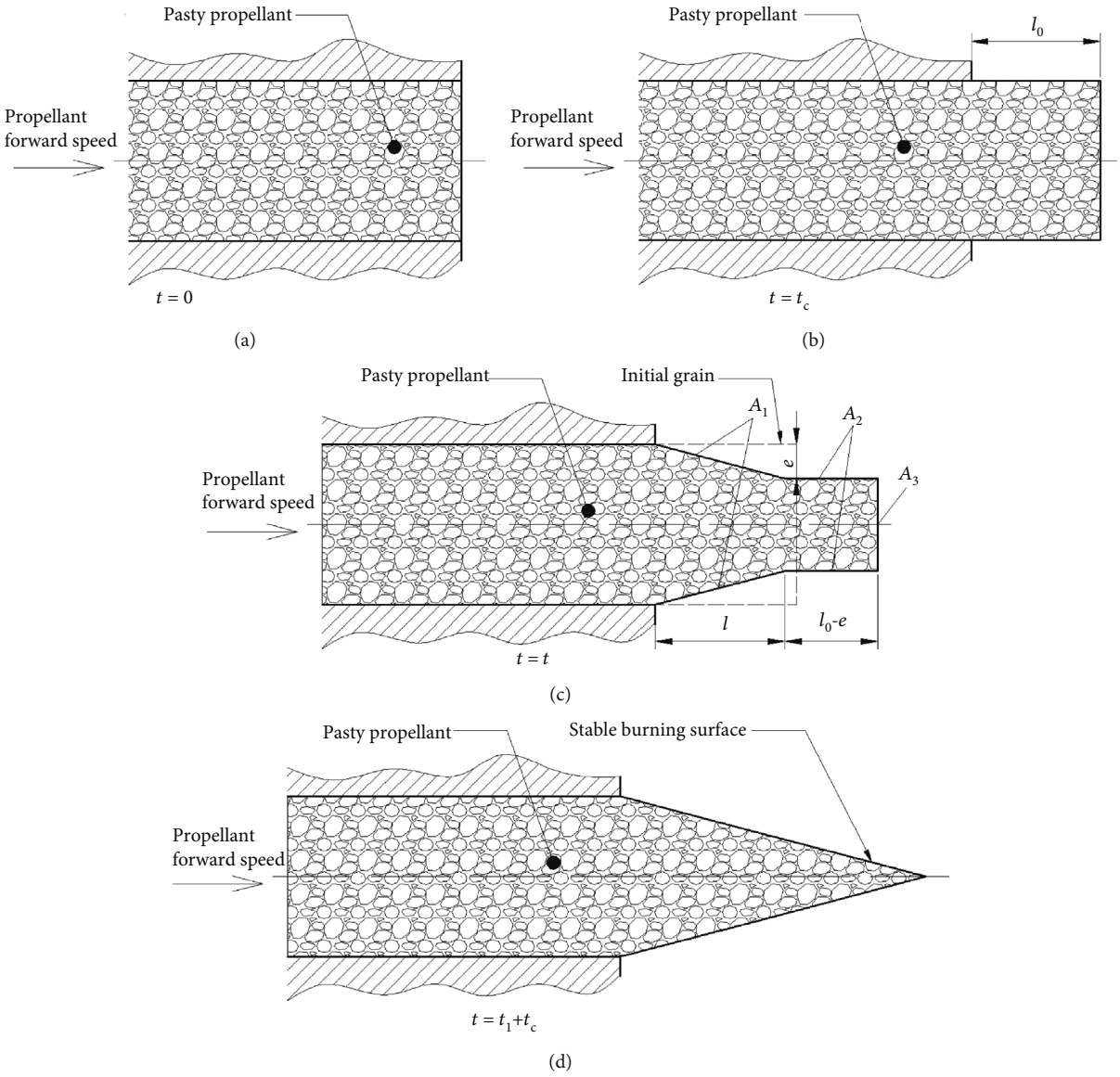

Figure 2: Burning surface change process of pasty propellant at the initial stage.

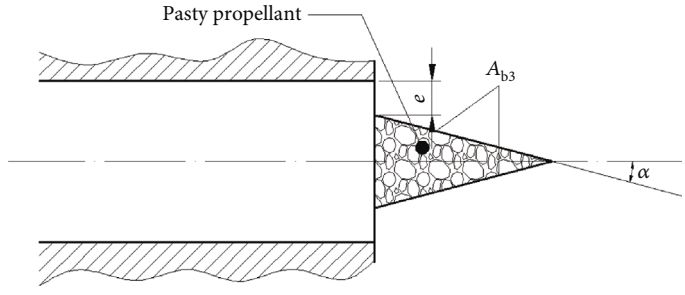

Figure 3: Burning surface of pasty propellant at the burning tail-off.

To analyze the entire burning surface change process of the pasty propellant in the combustion chamber, a cylinder grain of pasty propellant with the length of Δx at the exit of the transport pipeline is selected, as shown in Figure 1. The changing process of the burning surface with the movement of the selected grain consists of two parts, the retreat of the burning surface and the forward flow of propellant. The burning surface of the grain retreats in the radial direction

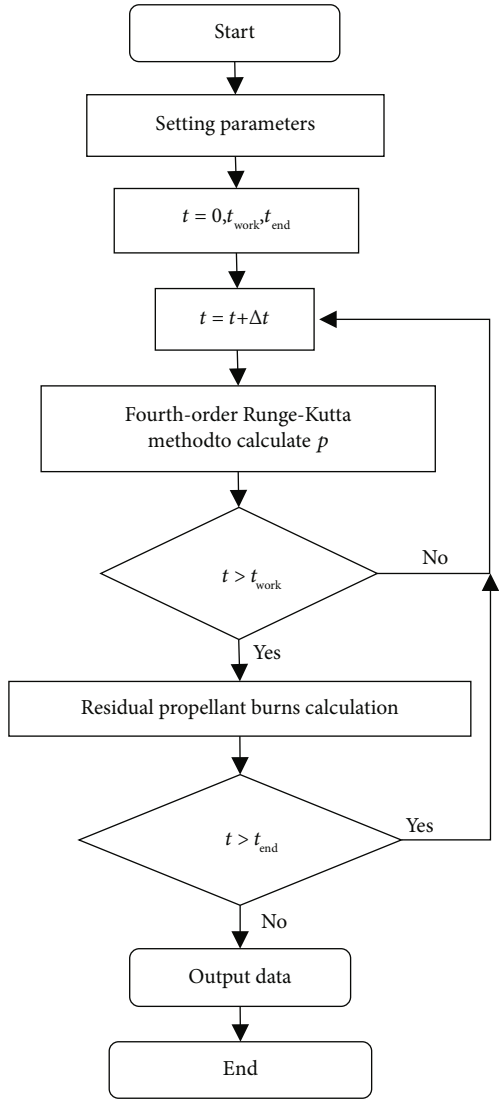

Figure 4: Computational flow chart for the internal ballistics of a pasty rocket engine.

due to the combustion of pasty propellant with the retreating speed of the propellant burning rate $\dot{r}$. The pasty propellant flow in the axial direction with the velocity of v is pushed by the hydraulic cylinder piston. The time when the front end of propellant flows through the pipeline exit is recorded as t_0'; then, after a certain time interval $\Delta t = t_1' - t_0'$, the position and geometric shape of the selected grain will change. The distance moves forward of the selected grain is $l = v\Delta t$, and the burned propellant web thickness is $e = \dot{r}\Delta t$. The movement speed of the propellant grain burning surface is $v_d = \sqrt{v^2 + \dot{r}^2}$. The motion tracking is an oblique straight line and the angle between the motion direction and the horizontal direction is $\alpha = \arctan(\dot{r}/v)$. In addition, when the burned propellant web thickness e is equal to $d/2$, the selected grain is completely burned, and the burning surface moving process of the selected grain can be considered as a cone, as shown by the dashed line in Figure 1. The bottom diameter of the cone is the diameter d of the pipeline, and the height h of the cone can be calculated by

$$h = v\left(t_2' - t_0'\right) = \frac{vd}{2\dot{r}}. \tag{11}$$

2.3. Burning Surface Equation of the Pasty Propellant. Similar to the solid propellant rocket motor, we can also divide the burning process of the pasty propellant rocket engine into three stages: initial burning stage, steady burning, and burning tail-off. The cone-shaped burning surface model is used to derive the burning surface equation of the pasty propellant in each working stage.

2.3.1. Initial Burning Stage. The pasty propellant burning process involves very complex physical and chemical combustion phenomena. Both the ignition gas spreading and the propellant surface reaction can lead to the ignition delay of the pasty rocket engine. During this period, the pasty propellant will accumulate at the outlet of the transportation pipeline. This part of the propellant is called the initial accumulation of pasty propellant. The initial accumulation of the pasty propellant is approximately cylindrical, and the cylindrical bottom is the end face of the outlet of the transport pipeline, and the height of the cylinder is $l_0 = vt_c$; t_c is the ignition delay time. After the accumulated pasty propellant is ignited, the combustion chamber is filled with high-temperature gas, and the pasty propellant squeezed out of the transport pipe will be ignited.

The ignition delay time t_c measured in the experimental test is 0.08~0.16 s, and the initial stacking length l_0 of the propellant is estimated to be 16~32 mm. In the initial combustion section, the shape of the pasty propellant burning surface is divided into two parts. The first part of the pasty propellant burning surface is cylindrical, and the other part is a frustum of the cone due to the burning of the propellant extruded from the transport pipeline. The burning surface of the pasty propellant is composed of three parts, namely, a conical side surface A_1, a cylindrical side surface A_2, and a cylindrical end surface A_3, as shown in Figure 2. The total burning surface area A_{b1} in this stage is calculated as

$$\begin{aligned} A_{b1} = N(A_1 + A_2 + A_3) = N\left(\pi\left(\frac{d}{2} + \frac{d}{2} - e\right)\sqrt{e^2 + l^2}\right. \\ \left. + \pi(d - 2e)(l_0 - e) + \pi\left(\frac{d}{2} - e\right)^2\right), \end{aligned} \tag{12}$$

where d is the diameter of the transport pipeline, e is the burned propellant web thickness, N is the number of transport pipelines, and l is the flow length of the propellant.

2.3.2. Steady Burning Segment. When the burned propellant web thickness is equal to the radius of the pipeline ($e = d/2$), the pasty propellant reaches a steady burning stage. The pasty propellant is continuously supplied from the tank by the hydraulic cylinder piston, which is equivalent to countless small grains entering into the combustion chamber one by one; thus, a complete cone formed as shown in Figure 2(d). Therefore, the burning surface of the pasty

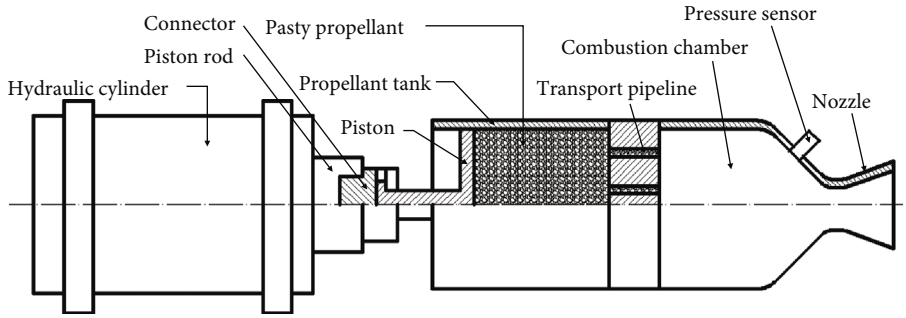

Figure 5: The schematic diagram of the laboratory-scale test pasty rocket engine.

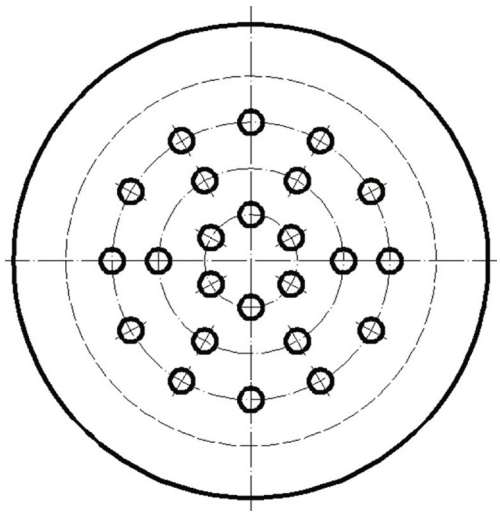

Figure 6: The schematic diagram of the transport pipeline distribution.

propellant is a cone-side surface. The burning surface area A_{b2} is

$$A_{b2} = N\pi \frac{d}{2} \sqrt{\left(\frac{d}{2}\right)^2 + h^2}, \tag{13}$$

where h is the height of the cone, as seen in equation (11).

2.3.3. Burning Tail-Off. When the supply of the pasty propellant is stopped, and residual propellant is burned following the geometrical burning law, which is similar to the solid rocket motor, the burning surface of pasty propellant in the burning tail-off is shown in Figure 3. It can be computed by

$$A_{b3} = \frac{N\pi((d/2) - e)}{\sin \alpha}, \tag{14}$$

where α is the half-apex angle of the cone.

To solve differential equation (10), the fourth-order Runge-Kutta method [25] is used to calculate the pressure evolution in the combustion chamber, as shown in Figure 4.

3. Experiment Instruments

In order to validate the present burning surface model, experiments were carried out on a laboratory-scale test pasty rocket engine. Figure 5 shows the schematic of the test pasty rocket engine, which consists of a hydraulic system, piston, propellant tank, transport pipeline, combustion chamber, nozzle assembly, and pressure measurement equipment. The hydraulic system is used to supply the pasty propellant with a large driving force up to 9 MPa and a wide adjustment range. The supply flow rate of the pasty propellant can be controlled by the foreword velocity of the hydraulic cylinder piston rod. The pasty propellant tank is filled with propellant, and the pasty propellant enters into the combustion chamber through transport pipelines. The tank diameter is 160 mm, and the length of the pasty propellant tank is 300 mm. The designed pasty rocket engine operation time is 1 s. The transport pipelines are straight round pipes, which are distributed according to a certain law, as shown in Figure 6. The diameter and length of the combustor are 128 mm and 134 mm, respectively. The diameter of the nozzle throat is 16.9 mm, and the black powder is used to ignite the pasty propellant. Figure 7 presents the photographic view of the pasty rocket experimental systems.

When the control system issues an ignition command, and the hydraulic system starts pushing the piston at the same time. The pasty propellant, which is driven by the piston, enters the combustion chamber through the transport pipeline. It is ignited by hot gas generated from the black powder. The control system issues a termination command after the engine works for a certain period, and the hydraulic system stops working. Then, the pasty propellant supply stops, which is marked as the end of the pasty rocket engine. The combustion chamber pressure evolutions are obtained by the test acquisition. The pasty propellant used in this paper is produced by Xi'an Modern Chemistry Research Institute, and the general components of the pasty propellant are listed in Table 1.

Table 2 summarizes the experimental case studied in this paper. $\dot{m}$ represents the mass flow rate of the pasty propellant. d, d_p, and d_t are the diameter of the transport pipeline, the propellant tank, and nozzle throat, respectively. N is the number of transport pipelines. v represents the velocity of the pasty propellant through the transport pipeline. v_p is

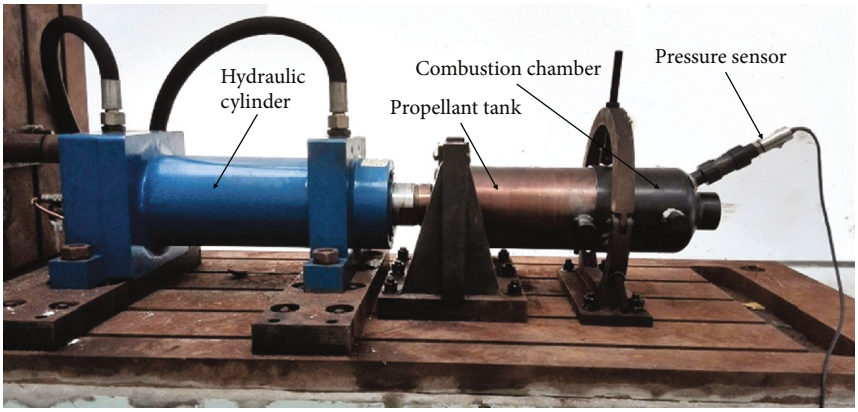

Figure 7: Photographic view of the pasty rocket engine test system.

Table 1: The general components of the pasty propellant ingredient.

Components	AP	HTPB	Al and B	Others
Type	Oxidizing agent	Polymer binder	Metal combustion agent	Curing agent, adhesive, etc.
Mass fraction	70.0 wt%	10.0 wt%	5.0 wt%	15.0 wt%

Table 2: Parameters used in the experiment.

Parameters	$\dot{m}$ (kg)	d_p (mm)	v_p (mm/s)	d (mm)	N	v (mm/s)	d_t (mm)	A_p/A_t
Value	0.5	160	14.4	8.0	24	240	16.9	5.376

Table 3: Physical parameters for the simulation of pressure evolution in the combustion chamber.

Parameter	Value
Specific heat ratio of the propellant gas γ	1.266
Gas constant of the propellant gas R_g	278.31 J/(kg·K)
Propellant adiabatic flame temperature T_p	2851 K
Propellant density ρ_p	1726 kg/m^3
Burning rate exponent of the propellant n	0.398
Burning rate coefficient of the propellant a	5.4×10^{-5} m/$(s \cdot \mathrm{Pa}^n)$

the velocity of the piston, and A_p/A_t is the ratio of pipe outlet area to the nozzle throat area.

4. Results and Discussion

4.1. Internal Ballistics of the Pasty Propellant Rocket Engine. The combustion chamber pressure evolutions of the pasty propellant rocker engine are simulated based on the zero-dimensional internal ballistic equation and burning surface change model described above. The diameter of the pipelines is $d = 8$ mm, the number of transport pipelines is $N = 24$, and the flow velocity of the pasty propellant is 240 mm/s, as listed in Table 2. The physical parameters of the pasty propellant used in the present study are listed in Table 3.

Figure 8 illustrates the pressure histories in the combustion chamber for both experimental data and calculated results. It can be seen from the experimental data that there is an obvious ignition delay that appeared in the ignition stage, and the delay is mostly due to the time required to heat the cold propellant until ignition occurs. After the delay time period t_c, the pressure trace increased quickly, then reached a stable value, and finally decreased. To analyze the internal ballistic characteristics of the pasty rocket engine, the pressure trace can be divided into three successive stages, namely, the ignition transient, steady burning segment, and the burning tail-off. When the pasty propellant is ignited and the engine starts to work, the pressure in the combustion chamber climbed quickly and then rapidly decreased to a stable value after reaching the initial pressure peak value p_m, which is defined as ignition transient t_1. The initial pressure peak occurs due to the ignition delay of the pasty propellant. The accumulated propellant resulted in a larger initial burning surface, which leads to the appearance of the initial pressure peak. This is different from the traditional solid rocket motor, whose initial pressure peak is induced mainly by erosion burning. In the steady burning stage, the pasty propellant maintains an almost constant burning surface, and this period is denoted as t_p. In the burning tail-off, the pasty

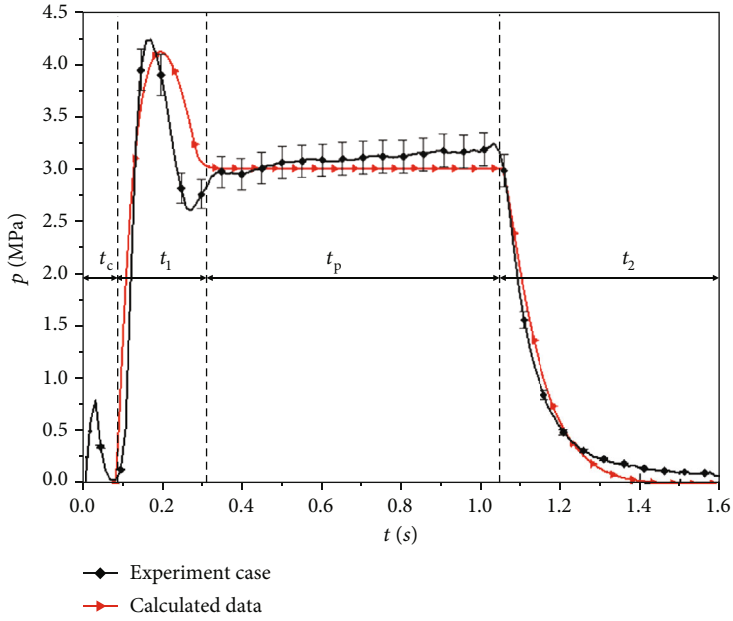

Figure 8: Time histories of the pressure in the combustion chamber for experimental data and calculated result.

Table 4: Comparison of internal ballistic parameters between experiment and calculation.

	p_{eq} (MPa)	p_m (MPa)	t_c (s)	t_1 (s)	t_p (s)	t_2 (s)
Experimental case	3.12	4.23	0.08	0.24	0.72	0.56
Calculated data	3.00	4.06	—	0.22	0.74	0.36

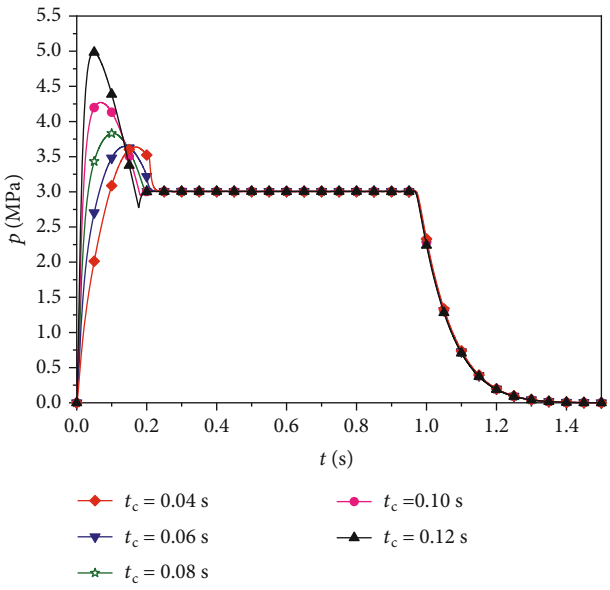

Figure 9: The pressure evolution in the combustor for different ignition delay times.

propellant stops supplying, and the residual propellant burns with a specific geometry. The pressure in the combustion chamber decreases rapidly, and this period is represented by residual burning time period t_2.

In addition, it can be seen from Figure 8 that the calculated value of the pressure in the combustion chamber is in good agreement with the data obtained by the experiment. Table 4 shows the parameters of the experimental and calculated values of the pressure history, and the deviation of the initial pressure peak is around 4.02%, which indicates that the simplification made in the burning surface model is reasonable.

4.2. Effect of the Ignition Delay Time. The effect of the ignition delay time on the internal ballistics of the pasty propellant rocket engine was also studied. Five different values of the ignition delay time t_c were employed, namely, $t_c = 0.04$ s, 0.06 s, 0.08 s, 0.10 s, and 0.12 s. The diameter of the pipelines is $d = 8$ mm, and the number of transport pipelines is $N = 24$. The free volume of the pasty rocket engine combustor is $V_g = 0.8 \times 10^{-3}$ m^3, and the flow velocity of the pasty propellant is 240 mm/s.

The calculated pressure evolutions in the combustor for different ignition delay times are shown in Figure 9. It can be noted that the evolutions of the pressure are qualitatively similar for all cases. The ignition delay time t_c has a significant effect on the initial burning stage and the initial pressure spike p_m. The pressure evolution exhibits little discrepancy for the equilibrium burning stage and the burning tail-off. For the different five ignition delay time cases, the calculated peak pressures p_m in the combustion chamber are 3.63, 3.64, 3.83, 4.27, and 4.99 MPa, respectively. The mean pressure rise rates in the initial burning stage for ignition delay time of 0.04 s, 0.06 s, 0.08 s, 0.10 s, and 0.12 s are 21.5 MPa/s, 26.9

MPa/s, 37.1 MPa/s, 62.7 MPa/s, and 102.0 MPa/s, respectively. The peak value p_m of the initial pressure grows by 37.5%, and the ignition transient t_1 reduces by 29.2% with the increase of ignition delay time. This is because that as the ignition delay time increases, the initial accumulation of pasty propellant and the initial burning surface area becomes larger during ignition, leading to an increase in the initial pressure peak as mentioned before. Therefore, the internal ballistic characteristics of the pasty propellant rocket engine can be improved by increasing the ignition powder or improving the formulation of the pasty propellant to reduce the ignition delay time.

4.3. Effect of the Transport Pipeline Structure. In order to study the influence of the transport pipeline structure on the internal ballistic characteristics, several values of transport pipeline diameter d and transport pipe number N were considered (d = 11.3 mm, 9.8 mm, 8.8 mm, 8.0 mm, and 7.4 mm and N = 12, 16, 20, 24, and 28) while the mass flow rate of pasty propellant was held constant. The free volume of the pasty rocket engine combustor is $V_g = 0.8 \times 10^{-3}$ m^3, the flow velocity of the pasty propellant is 240 mm/s, and the ignition delay time is set to 0.08 s.

Figure 10 illustrates the pressure evolutions in the combustor for different transport pipeline structures, while the values of the peak pressure p_m, ignition transient t_1, steady burning time period t_p, and residual propellant burning time period t_2 are shown in Table 5. Note that the number and diameter of the transport pipe have a significant influence on the initial rapid pressurization, steady burning time period, and pressure drop process of the pasty rocket engine, while has little effect on the equilibrium pressure. As the transport pipe number increases (or the transport pipe diameter decreases), the initial pressure peak value and steady burning time period increase acutely, while the ignition transient is significantly reduced. When the transport pipe number changes from 12 to 28, the steady burning time period t_p increases by 17.6%. However, the ignition transient t_1 and residual propellant burning time period t_2 decrease by 41.4% and 34.0%, respectively.

In the rapid rise of the initial pressure, the mean pressure rise rates for transport pipe numbers of 12, 16, 20, 24, and 28 are 18.0 MPa/s, 23.6 MPa/s, 30.0 MPa/s, 37.1 MPa/s, and 45.4 MPa/s, respectively. It is because that to keep a constant mass flow rate, a larger transport pipeline number comes with a smaller transport pipeline diameter, which increases the total initial burning surface area and causes the pressure to rise rapidly. With the increase of transport pipe number, the residual burning time becomes shorter while a relatively small discrepancy of the pressure descent rate is observed. This is due to that the burning time of the residual propellant can be approximately calculated by $t_2 = d/2\dot{r}$. Hence, when the mass flow rate of pasty propellant is held constant, the transport pipeline structure can affect not only the pressure spike of the initial burning stage but also the time period of the steady burning stage.

4.4. Effect of Free Volume of the Combustion Chamber. A parameter which can have a significant effect on the internal ballistics of the pasty propellant rocket engine is the free volume of the combustion chamber. A limited study of this effect is also carried out here, and several values of free volume V_g are considered, namely, $V_g = 0.4 \times 10^{-3}$ m^3, 0.8×10^{-3} m^3, 1.2×10^{-3} m^3, 1.6×10^{-3} m^3, and 3.2×10^{-3} m^3. The diameter and number of the transport pipeline are set to d = 8 mm and N = 24. The flow velocity of the pasty propellant is 240 mm/s, and the ignition delay time is set to 0.08 s.

Figure 11 shows the pressure evolutions in the combustor for different free volume of combustion chamber. Table 6 summarizes the numerical values of the peak pressure p_m and initial combustion time t_1 under the four operating conditions. It can be seen from Figure 11 that the free volume of the combustion chamber has a great effect on the initial burning stage of the pasty rocket engine but has little effect on the equilibrium burning segment and burning tail-off. With the increase of free volume V_g of the combustion chamber, the initial pressure spike p_m increased and the time to reach the equilibrium pressure increased. For a large free volume of the combustor, the equilibrium time period t_p is reduced. It is obvious that the smaller the free volume of the combustion chamber, the faster the pressure of the

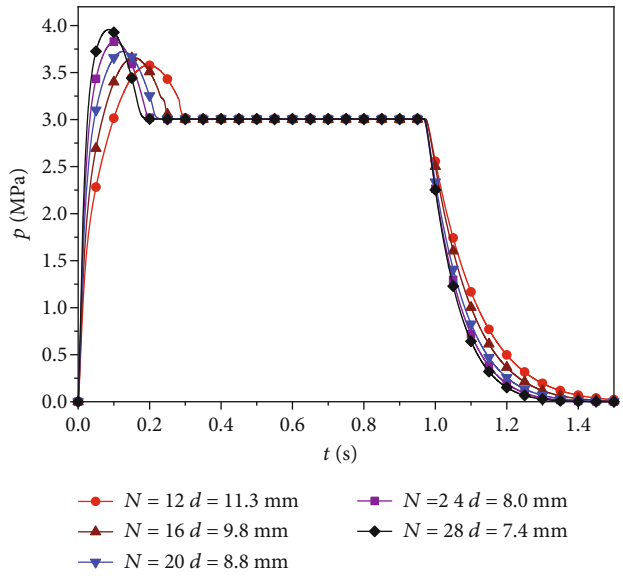

Figure 10: The pressure evolutions in the combustor for different transport pipeline structures.

Table 5: Calculated results of internal ballistic characteristics for different structures of transport pipeline.

N	d (mm)	p_m (MPa)	t_1 (s)	t_p (s)	t_2 (s)
12	11.3	3.57	0.29	0.68	0.53
16	9.8	3.66	0.25	0.72	0.46
20	8.8	3.72	0.21	0.76	0.40
24	8.0	3.83	0.19	0.78	0.38
28	7.4	3.96	0.17	0.80	0.35

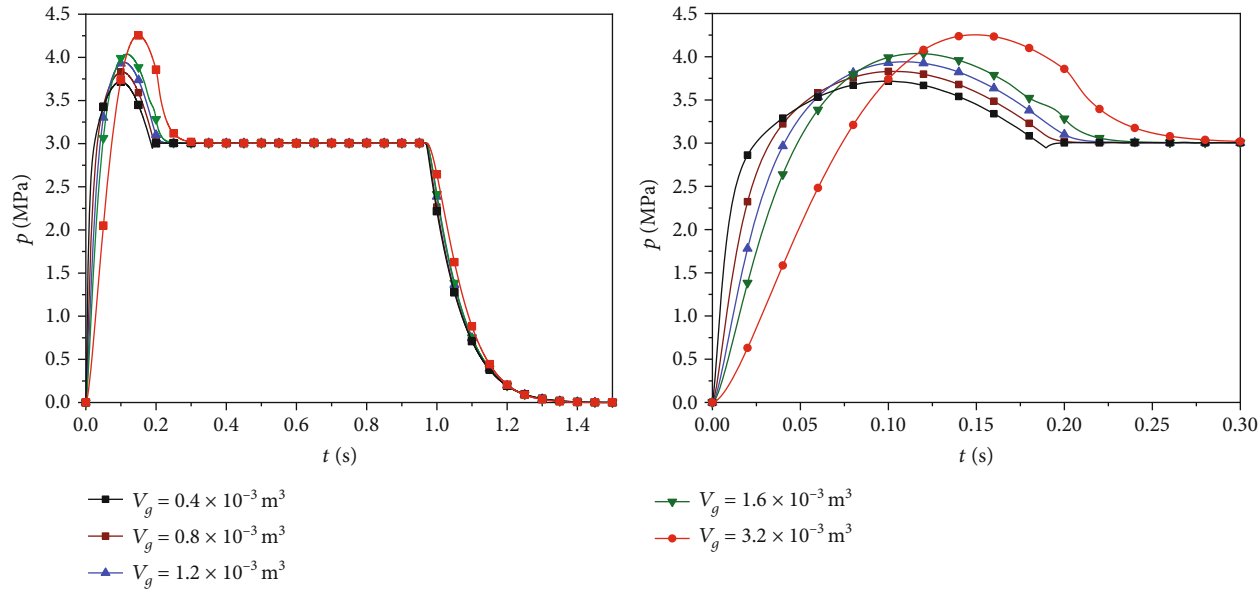

Figure 11: The pressure evolutions in the combustor for different free volume of combustion chamber.

Table 6: Calculated results of p_m and t_1 for different free volume of the combustion chamber.

V_g (10^{-3} m^3)	p_m (MPa)	t_1 (s)	t_p (s)
0.4	3.72	0.18	0.79
0.8	3.83	0.19	0.78
1.2	3.94	0.23	0.74
1.6	4.04	0.25	0.72
3.2	4.26	0.30	0.67

combustion chamber rises. The calculated pressure peak ratio increases from 1.24 to 1.42 with an increase of the free volume of the combustion chamber, and the time to achieve the equilibrium pressure increases from 0.18 s to 0.30 s. The reason for this phenomenon is that the decrease of the free volume of the combustion chamber will cause an increase in the pressure rise rate of the combustion chamber. While the burning rate of the pasty propellant has an exponential relationship with the pressure, so the average burning rate reaching the equilibrium segment increases, and the time to reach the equilibrium stage is reduced. Therefore, the free volume of the combustion chamber should be reduced so that the remnant of propellant due to incomplete combustion could be minimized.

4.5. Effect of Mass Flow Rate of the Propellant. Five different mass flow rates of the pasty propellant were taken into consideration here to study the effect of mass flow rate on the internal ballistic characteristics of the pasty rocket engine. The mass flow rates $\dot{m}$ of the pasty propellant are 0.08 kg/s, 0.25 kg/s, 0.50 kg/s, 0.75 kg/s, and 1.00 kg/s, and the number of the transport pipeline N is 4, 12, 24, 36, and 48, respectively. The flow velocity of the pasty propellant v is 240 mm/s, and the ignition delay time t_c is set to 0.08 s. The diameter of the pipeline is $d = 8$ mm, the free volume of the pasty rocket engine combustor is $V_g = 0.8 \times 10^{-3}$ m^3, and we change the nozzle throat diameter to keep the equilibrium pressure of the combustion chamber at 3 MPa. The calculated pressure evolutions in the combustor for mass flow rate are shown in Figure 12.

As can be seen from Figure 12, the mass flow rate of the pasty propellant has a great effect on the initial burning stage of the pasty rocket engine and has little effect on the equilibrium burning stage and burning tail-off. The mean pressure rise rates increase while the initial pressure spike decreased with an increase of the mass flow rate of the pasty propellant.

It is obvious that when the mass flow rate $\dot{m} = 0.08$ kg/s, the pressure in the combustion chamber rises slowly after the engine is ignited. The initial pressure peak p_m reached 4.31 MPa, and the time to reach the equilibrium period t_1 is 0.36 s. When the mass flow rate $\dot{m} = 1.00$ kg/s, the pressure in the combustion chamber rises quickly. The pressure peak is small, only 3.72 MPa, and the time to reach the equilibrium stage is 0.18 s. Table 7 lists the calculation results in each case. Therefore, we can conclude that the lower the mass flow rate, the slower the combustion chamber pressure rises, the higher the pressure peak, and the longer it takes to reach the equilibrium period. We should appropriately increase the mass flow rate of the pasty propellant when designing the rocket engine to obtain better internal ballistic performance.

4.6. Effect of the Flow Velocity of the Pasty Propellant. The effect of the flow velocity of the pasty propellant on the internal ballistics of the pasty propellant rocket engine was also studied. Different flow velocities v from 180 mm/s to 360 mm/s were taken into consideration to study this effect. The diameter and number of the transport pipeline are set

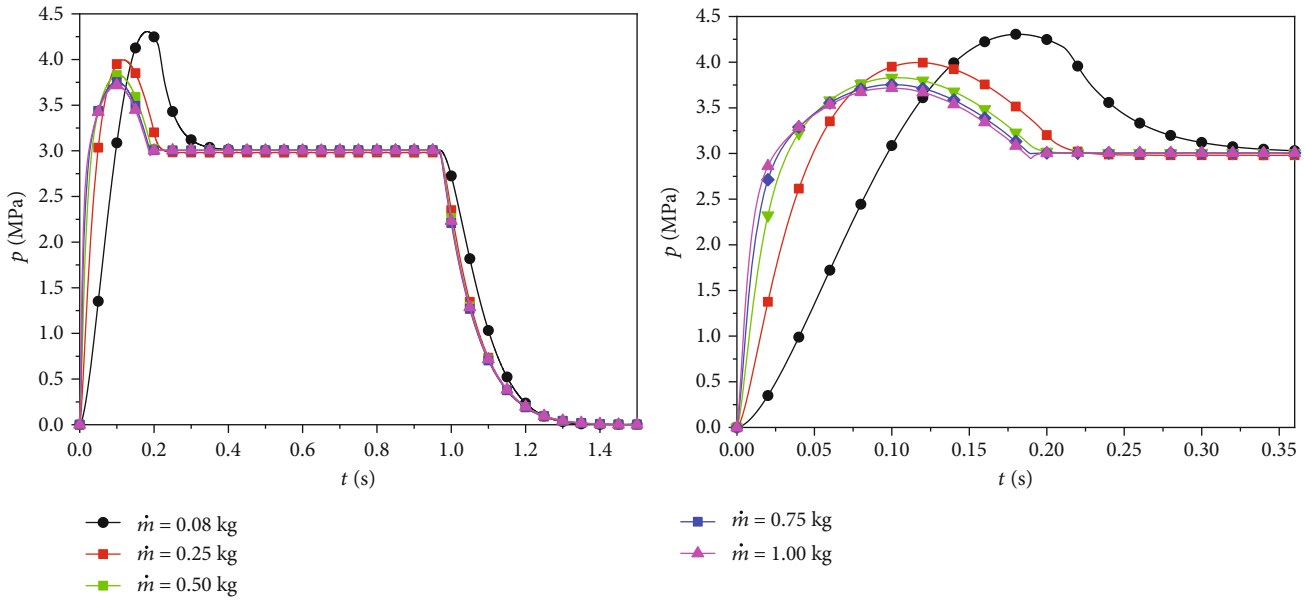

Figure 12: The pressure evolutions in the combustor for different mass flow rate of the pasty propellant.

Table 7: The main parameters calculated results for different mass flow rates of the pasty propellant.

Parameters	$\dot{m}$ (kg/s)	N	d_t (mm)	p_m (MPa)	t_1 (s)
Value	0.08	4	6.76	4.31	0.36
	0.25	12	12.0	4.00	0.26
	0.50	24	16.9	3.83	0.19
	0.75	36	20.7	3.75	0.19
	1.00	48	23.9	3.72	0.18

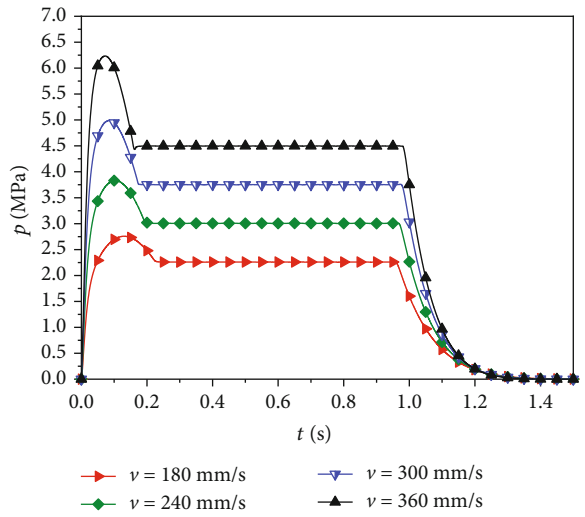

Figure 13: The pressure evolutions in the combustor for different flow velocities of the pasty propellant.

to $d = 8$ mm and $N = 24$, and the ignition delay time t_c is set to 0.08 s.

Figure 13 illustrates the pressure evolution trace with time for different flow velocities of the pasty propellant, and Table 8 lists the main parameters of the calculated results. Noted that the flow velocity of the pasty propellant has a significant influence on the initial rapid pressurization, initial pressure spike p_m, and the equilibrium pressure p_{eq}. In the rapid rise of the initial pressure, the mean pressure rise rates for flow velocities of 180 mm/s, 240 mm/s, 300 mm/s, and 360 mm/s are 21.3 MPa/s, 37.1 MPa/s, 58.4 MPa/s, and 85.8 MPa/s, respectively.

As shown in Figure 14, it is clear that the initial pressure spike p_m and equilibrium pressure p_{eq} increase linearly with the increase of the flow velocity v of the pasty propellant, while the increase rate of the initial pressure spike is greater than the increase rate of the equilibrium pressure. This is mostly due to higher propellant flow velocity leads to more initial accumulation of the pasty propellant. However, the ignition transient t_1 decreases with the increase of the pasty propellant flow velocity. When the flow velocity of the pasty propellant increases from 180 mm/s to 360 mm/s, the ignition transient t_1 decreases by 30.4%.

In addition, to study the thrust adjustment characteristics of the pasty rocket engine, the pasty propellant flow velocity is changed during the operation process. In this case, the initial flow velocity of the pasty propellant is $v = 240$ mm/s, and the flow velocity is set to $v = 120$ mm/s after the engine works for one second. Then, the flow velocity is $v = 360$ mm/s after one second. The calculated pressure evolution in the combustor with the variation of pasty propellant flow velocity is shown in Figure 15. As can be seen from Figure 15, obviously, the pressure in the combustion chamber changes with the flow velocity of the pasty propellant. When the flow velocity varies, the pressure in the combustion chamber responds quickly. Therefore, the pasty rocket engine thrust can be accurately adjusted by controlling the flow velocity of the pasty propellant.

Table 8: The main parameters calculated results for different flow velocities of the pasty propellant.

Parameters	v (mm/s)	v_p (mm/s)	N	d_t (mm)	p_m (MPa)	p_{eq} (MPa)	p_{eq}/p_m	t_1 (s)
Value	180	10.8	24	16.9	2.76	2.26	1.22	0.23
	240	14.4	24	16.9	3.83	3.00	1.28	0.19
	300	18.0	24	16.9	4.99	3.75	1.33	0.18
	360	21.6	24	16.9	6.23	4.50	1.38	0.16

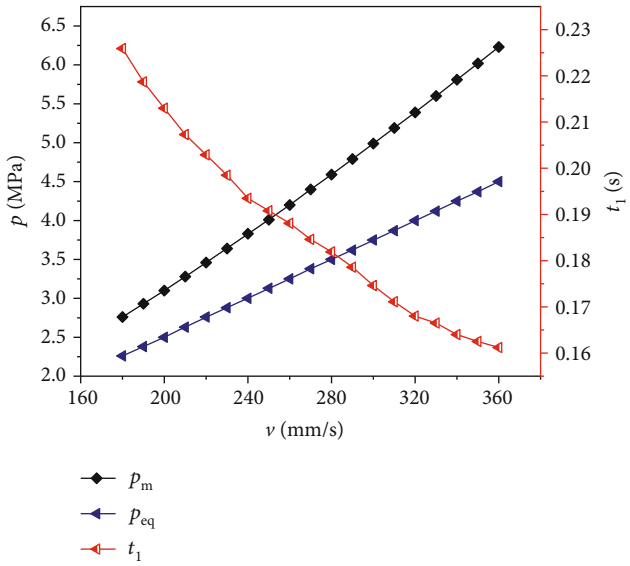

Figure 14: The pressure spike, equilibrium pressure, and ignition transient for different flow velocities of the pasty propellant.

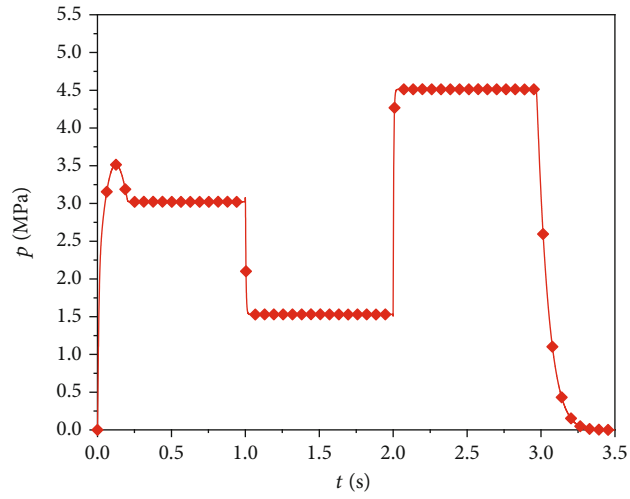

Figure 15: The pressure evolution in the combustor with the variation of pasty propellant flow velocity.

5. Conclusions

In this paper, the combustion characteristic of the pasty propellant is studied both experimentally and numerically. The program calculated results are in good agreement with the experimental data. In particular, the impact of ignition delay time, structure of the transportation pipe, free volume of the combustion chamber, and mass flow rate of the pasty propellant on the internal ballistic performance are analyzed. Conclusions are summarized as follows:

(1) During the stable operation of the pasty propellant rocket engine, the burning surface of the pasty propellant appears conical. The calculation model proposed in this paper is reasonable for the calculation of the internal ballistic characteristic parameters of the pasty propellant rocket engine, and the error of the initial pressure peak is only 4.02%

(2) When the ignition delay time increased, the pressure peak raised faster. However, the value of the initial pressure peak in the combustion chamber increases with the increase of the ignition delay time due to the accumulation of the pasty propellant. As the diameter of the transport pipeline decreases, the initial burning time and residual propellant burning time of the engine become shorter. The transport pipe diameter changes from 11.3 mm to 7.4 mm, and the initial combustion time and residual propellant combustion time decreased by 41.3% and 36.0%

(3) The reduction of the free volume of the combustion chamber can reduce the initial pressure peak of the pasty propellant rocket engine and the time to reach the equilibrium pressure. Therefore, the free volume of the combustion chamber should be reduced to control the remnant portion of the propellant

(4) The larger mass flow rate of the pasty propellant makes the combustion chamber pressure rise faster and can reduce both the initial pressure peak and the time to reach the equilibrium in the combustion chamber. The initial pressure spike and equilibrium pressure increase linearly with the increase of the flow velocity of the pasty propellant while the ignition transient decreased with the increase of the pasty propellant flow velocity

For further study, experiments can be conducted to study the influence of the pasty propellant flow velocity changes on internal ballistics and obtain the shape of the pasty propellant grains during the burning process. The two-phase flow of the pasty propellant can also be studied.

Nomenclature

a: Burning rate coefficient of propellant, m/(s·MPa^n)
A_b: Propellant burning surface area, m^2

A_t: The nozzle throat area, m^2
C^*: Characteristic velocity, m/s
d: Transport pipe diameter, m
e: The web thickness burned, m
h: The height of the cone, m
l: The distance moves forward, m
l_0: The initial stacking length, m
$\dot{m}$: The mass flow rate of the pasty propellant, kg/s
$\dot{m}_r$: The gas mass change rate in the combustion chamber, kg/s
$\dot{m}_b$: The combustion gas generation rate, kg/s
$\dot{m}_0$: The mass flow rate of the gas discharged through the nozzle, kg/s
n: Burning rate exponent of propellant
N: Number of the transport pipe
p: Pressure in combustion chamber, MPa
p_{eq}: Equilibrium pressure, MPa
p_m: Initial pressure peak, MPa
$\dot{r}$: Propellant burning rate, m/s
R_g: The combustion gas constant, J/(kg·K)
t_c: The ignition delay time, s
t_1: Initial burning time, s
t_p: Steady burning time, s
t_2: Residual burning time, s
T: Temperature in combustion chamber, K
v: Velocity of the pasty propellant flow forward, m/s
v_p: Velocity of the piston rod, m/s
v_d: Velocity of the grain surface move, m/s
V_g: The free volume of the combustion chamber, m^3
α: The angle between the speed direction and the horizontal
γ: Specific heat ratio of gas
ρ_g: Density of combustion gas, kg/m^3
ρ_p: The pasty propellant density, kg/m^3.

Data Availability

The data used to support the findings of this study are included within the article.

Conflicts of Interest

The authors declare that they have no conflicts of interest.

Acknowledgments

This research was supported by the National Natural Science Foundation of China (No. 52006099), the Fundamental Research Funds for the Central Universities (No. 30920021102 and No. 309181B8812), and the Six Talent Peaks Project in Jiangsu Province of China (No. 2016-HKHT-017).

References

[1] R. H. Frisbee, "Advanced propulsion for the XXIst century," in *AIAA International Air and Space Symposium and Exposition*, Dayton, Ohio, 2003.

[2] A. M. Ivanchenko, S. G. Bondarenko, Y. Protsan, and S. A. Wilson, "Deep regulation and reusable rocket propulsion using premixed slurry propellant," *Journal of Propulsion and Power*, vol. 28, no. 5, pp. 869–875, 2012.

[3] W. K. Yasuhara, A. Olson, and S. Finato, "Advanced gel propulsion controls for kill vehicles," in *Annual Interceptor Technology Conference*, Albuquerque, NM, USA, 1993.

[4] H. K. Ciezki, J. Hürttlen, K. W. Naumann, M. Negri, J. Ramsel, and V. Weiser, "Overview of the German gel propulsion technology program," in *50th AIAA/ASME/SAE/ASEE Joint Propulsion Conference*, Cleveland, OH, 2014.

[5] V. Kukushkin, "State and prospects of solid propellant rocket development," in *28th Joint Propulsion Conference and Exhibit*, Nashville, TN, USA, 1992.

[6] V. Kukushkin and A. Ivanchenko, "The pasty propellant rocket engine development," in *29th Joint Propulsion Conference and Exhibit*, Monterey, CA, USA, 1993.

[7] M.-D. Song and D.-Y. Ye, "Study of a new pasty propellant multi-purpose rocket motor," in *34th AIAA/ASME/SAE/ASEE Joint Propulsion Conference and Exhibit*, Cleveland, OH, USA, 1998.

[8] J. X. Zhang, Y. T. Ju, S. Q. Zhou, and C. Zhou, "Air-pasty propellant pressure drop and heat transfer through round pipe," in *2008 Asia Simulation Conference - 7th International Conference on System Simulation and Scientific Computing*, pp. 1282–1285, Beijing, China, 2008.

[9] Y. Luo, Y. Xing, X. Liu, and C. Liang, "Thermal structure analysis and simulation of solid-gelled propellant gas generator," *Journal of Beijing University of Aeronautics and Astronautics*, vol. 44, no. 8, pp. 1772–1779, 2018.

[10] C. H. Liu, F. Feng, and Q. L. Cao, "Study on starts of pasty propellant gas generator," *Journal of Propulsion Technology*, vol. 39, no. 2, pp. 374–379, 2018.

[11] B. Natan and S. Rahimi, "The status of gel propellants in year 2000," *International Journal of Energetic Materials and Chemical Propulsion*, vol. 5, no. 1-6, pp. 172–194, 2002.

[12] C. R. Douglas and L. Z. Rober, "Characterization of aluminum/RP-1 gel propellant properties," in *24th Joint Propulsion Conference*, Boston, MA, USA, 1988.

[13] K. Hodge, T. Crofoot, and S. Nelson, "Gelled propellants for tactical missile applications," in *35th Joint Propulsion Conference and Exhibit*, Los Angeles, CA, USA, 1999.

[14] S. R. Turns and D. C. Mueller, "Ignition and combustion characteristics of metallized propellants," Semi-Annual Report, Grant No. NAG 3-1044, 1990.

[15] D. C. Mueller and S. R. Turns, "Ignition and combustion characteristics of metallized propellants - Phase II," Annual Report, NASA Lewis Research Center, Grant NAG 3–1044, 1994.

[16] S. Bondarenko, A. Dreus, and K. Lysenko, "The investigation of thermal and gas dynamic processes in the combustion chamber of the rocket engine using slurry fuel," *Proceedings of the Institution of Mechanical Engineers, Part G: Journal of Aerospace Engineering*, vol. 232, no. 10, pp. 1903–1910, 2018.

[17] S. Rahimi, D. Hasan, and A. Peretz, "Development of laboratory-scale gel propulsion technology," *Journal of Propulsion and Power*, vol. 20, no. 1, pp. 93–100, 2004.

[18] Q.-L. Cao, W.-H. Liao, W.-T. Wu, and F. Feng, "Combustion characteristics of inorganic kerosene gel droplet with fumed silica as gellant," *Experimental Thermal and Fluid Science*, vol. 103, pp. 377–384, 2019.

[19] Q.-L. Cao, M. Massoudi, W.-H. Liao, F. Feng, and W.-T. Wu, "Flow characteristics of water-HPC gel in converging tubes and tapered injectors," *Energies*, vol. 12, no. 9, 2019.

[20] Q.-L. Cao, W.-T. Wu, W.-H. Liao, F. Feng, and M. Massoudi, "Effects of temperature on the flow and heat transfer in gel fuels: a numerical study," *Energies*, vol. 13, no. 4, 2020.

[21] N. Yilmaz, B. Donaldson, W. Gill, and W. Erikson, "Solid propellant burning rate from Strand burner pressure measurement," *Propellants, Explosives, Pyrotechnics*, vol. 33, no. 2, pp. 109–117, 2008.

[22] S. M. Davis and N. Yilmaz, "Thermochemical analysis of hypergolic propellants based on triethylaluminum/nitrous oxide," *International Journal of Aerospace Engineering*, vol. 2014, Article ID 269836, 5 pages, 2014.

[23] A. M. Tahsini and K. Mazaheri, "Internal ballistics simulation of SRM's: viscous terms effects," in *42nd AIAA/ASME/SAE/ASEE Joint Propulsion Conference & Exhibit*, Sacramento, California, 2006.

[24] D. R. Greatrix, "Parametric evaluation of solid rocket motor internal ballistics," in *46th AIAA/ASME/SAE/ASEE Joint Propulsion Conference & Exhibit*, Nashville, TN, 2010.

[25] M. A. Willcox, M. Q. Brewster, K. C. Tang, D. S. Stewart, and I. Kuznetsov, "Solid rocket motor internal ballistics simulation using three-dimensional grain burnback," *Journal of Propulsion and Power*, vol. 23, no. 3, pp. 575–584, 2007.

[26] W. Ki, T. Ko, S. Kim, and W. Yoon, "3D grain burnback analysis using the partial interface tracking method," *Aerospace Science and Technology*, vol. 68, pp. 58–67, 2017.

[27] C. Tola and M. Nikbay, "Solid rocket motor propellant optimization with coupled internal ballistic–structural interaction approach," *Journal of Spacecraft and Rockets*, vol. 55, no. 4, pp. 936–947, 2018.

[28] C. Tola and M. Nikbay, "Internal ballistic modeling of a solid rocket motor by analytical burnback analysis," *Journal of Spacecraft and Rockets*, vol. 56, no. 2, pp. 498–516, 2019.

[29] F. Qin, H. Guoqiang, L. Peijin, and L. Jiang, "Algorithm study on burning surface calculation of solid rocket motor with complicated grain based on level set methods," in *42nd AIAA/ASME/SAE/ASEE Joint Propulsion Conference & Exhibit*, Sacramento, California, 2006.

[30] C. Griego, N. Yilmaz, and A. Atmanli, "Sensitivity analysis and uncertainty quantification on aluminum particle combustion for an upward burning solid rocket propellant," *Fuel*, vol. 237, pp. 1177–1185, 2019.

[31] C. Griego, N. Yilmaz, and A. Atmanli, "Analysis of aluminum particle combustion in a downward burning solid rocket propellant," *Fuel*, vol. 237, pp. 405–412, 2019.

[32] N. Yilmaz, "Modeling of aluminum particle ignition behavior in open atmosphere rocket propellant fires," *Proceedings of the Institution of Mechanical Engineers, Part G: Journal of Aerospace Engineering*, vol. 230, no. 4, pp. 690–697, 2016.

[33] N. Yilmaz, J. Height, B. Donaldson, W. Gill, and F. Vigil, "Rocket motor exhaust thermal environment characterization," *Measurement*, vol. 122, pp. 312–319, 2018.

[34] M. J. Ward, S. F. Son, and M. Q. Brewster, "Role of gas- and condensed-phase kinetics in burning rate control of energetic solids," *Combustion Theory and Modelling*, vol. 2, no. 3, pp. 293–312, 1998.